Journal of Modern Optics
Publication details, including instructions for authors and subscription information:
http://www.tandfonline.com/loi/tmop20

Design of adaptive digital filters for phase extraction in complex fringe patterns obtained using the Ronchi test

Jesus Caum [a], Josep Arasa [a], Santiago Royo [a] & Miguel Ares [a]
[a] Center for Sensor, Instrumentation and Systems Development (CD6), Universitat Politècnica de Catalunya (UPC-Barcelona Tech), Rambla Sant Nebridi 10, E-08222 Terrassa, Spain

Available online: 15 Feb 2012

To cite this article: Jesus Caum, Josep Arasa, Santiago Royo & Miguel Ares (2012): Design of adaptive digital filters for phase extraction in complex fringe patterns obtained using the Ronchi test, Journal of Modern Optics, 59:8, 721-728

To link to this article: http://dx.doi.org/10.1080/09500340.2012.659767

Journal of Modern Optics
Vol. 59, No. 8, 10 May 2012, 721–728

Taylor & Francis
Taylor & Francis Group

Design of adaptive digital filters for phase extraction in complex fringe patterns obtained using the Ronchi test

Jesus Caum, Josep Arasa, Santiago Royo* and Miguel Ares

Center for Sensor, Instrumentation and Systems Development (CD6), Universitat Politècnica de Catalunya (UPC-Barcelona Tech), Rambla Sant Nebridi 10, E-08222 Terrassa, Spain

(*Received 12 October 2011; final version received 13 January 2012*)

A powerful technique is presented for processing complex fringe patterns with high noise levels and arbitrary distributions of spatial frequencies, which can successfully extract the phase information. Artifacts that arise from phase extraction in local filtering approaches are avoided by using a simple design and implementation strategy for the adaptive filter, based on the theory of digital filter design used in electronics, and applied to pixel rows (or columns) in the fringe-pattern. The filter designed in this manner is then applied to phase extraction in an experimental fringe pattern measured in a digital Ronchi test setup using a Carré phase-shifting procedure. The filtering strategy has a very low computational cost and allows phase extraction in noisy ronchigrams regardless their spatial frequency distribution, provided the fringes are still visible.

Keywords: optical metrology; Ronchi test; fringe analysis; signal processing

1. Introduction

Fringe patterns have become a valuable source of information in several optical metrology techniques, from interferometry to deflectometry and fringe projection. This has led digital fringe-pattern processing to become a key part of the complete metrology strategy of the technique used, as it is required for yielding the signal prepared for phase extraction [1], typically by use of phase-shifting algorithms [2] or by spatial carrier fringe-pattern analysis [3]. The generally accepted approach involves some signal-smoothing processing that simultaneously removes noise effects, so the signal is driven towards its desired sinusoidal shape, allowing accurate phase information to be extracted from the fringe pattern. However, in certain measurement techniques, the measurement strategy gives rise to a number of artifacts which make the signal depart from the sinusoidal shape required for phase-shifting strategies. In the case of the Ronchi test, where a grating of square transmittance is normally used to sample the wavefront [4], the diffractive effects introduced by the grating may prevent from using a phase-shifting scheme, as they are spatially dependent on the local curvature of the impinging wavefront [5].

A number of fringe-processing techniques have been proposed in the literature [6]. A very successful approach for fringe patterns that are spatially monochromatic is fringe transform profilometry, constructed using fast Fourier transform (FFT) filtering [7]. For fringe patterns which are locally monochromatic, a number of strategies have been proposed, such as using windowed Fourier transforms [8], Gabor filters [9] and wavelet transforms [10], among others. However, these filters present some drawbacks regarding its phase extraction results. Firstly, for signals of changing frequency the use of local windowing strategies for filtering, which depend on the position of the fringe in the image and on the local frequency of the fringe pattern, complicates the phase extraction procedure (notably the phase-unwrapping step) [11,12] due to the effects of the windowing procedure on the signal. Secondly, phase shifting schemes are not valid in the case of signals whose shape departs from the sinusoidal shape, and which, in addition, depart from it depending on the local curvature of the incident wavefront. These alterations locally disturb the accuracy of the measurement.

The method we present overcomes these drawbacks by applying a digital filter designed to match the spatial frequency distribution of each pixel row or column in the image. The filter is applied once in each direction, cancelling out the displacement of the fringes introduced by each pass of the filter. With this simple strategy, a low-order filter is enough to properly attenuate the high-order components of the fringe-pattern with a very low computational cost. The filter is valid for fringe patterns with any noise level and with

*Corresponding author. Email: royo@oo.upc.edu

ISSN 0950–0340 print/ISSN 1362–3044 online

http://dx.doi.org/10.1080/09500340.2012.659767
http://www.tandfonline.com

any distribution of spatial frequencies, and is general enough to be applied for phase extraction in any experimental technique yielding non-monochromatic fringe-patterns, even in the case the involved signals have a non-sinusoidal intensity distribution.

The paper is organized as follows. Section 2 gives a brief introduction to digital filter design theory while it discusses the methodology used for the adaptive filter design which will be implemented. In Section 3, the designed strategy is applied to a complex fringe pattern obtained using a digital Ronchi deflectometry setup [13,14], in which the properties of the filter are discussed in detail. Next, a phase extraction procedure using a classical Carré phase shifting algorithm is performed, showing the capability of the filter to allow phase extraction in complex fringe patterns. A comparison of the phase values obtained after applying to the same fringe pattern the proposed filtering strategy and a non-adaptive filtering strategy is shown, allowing the quantification of the associated measurement error. Section 4 discusses the main conclusions of our work.

2. Introduction to digital filter design

Digital filter theory is intended to work on the time-dependent signals used in electronics signal processing. It provides a general methodology for filter design which is relevant to the problem of fringe-pattern processing. In the fringe-pattern processing case, each line orthogonal to the fringes in the image may be interpreted as a periodic signal with an arbitrary distribution of spatial frequencies, determined by the size of the CCD array and of the individual pixels, and by the distribution of the fringes in the image. We aim to design a digital filter in the spatial domain based on the well-established set of procedures involved in digital filter design. Below, we briefly review the theory of digital filter design. Only the aspects most relevant to fringe pattern processing are presented, as plenty of high-quality literature is available on the topic [15–17].

2.1. Definitions

Our approach intends to reduce the high-frequency components (in spatial terms) of each pixel row or column in an image, which are processed in sequence until the entire fringe pattern has been analyzed. As a consequence we consider a low-pass digital continuous filter, in which the attenuation of the signal (δ_c) below the cut-off frequency (Ω_c) is small (typically fixed below 3 dB), and the attenuation δ_a after the minimum attenuated frequency (Ω_a) is very significant.

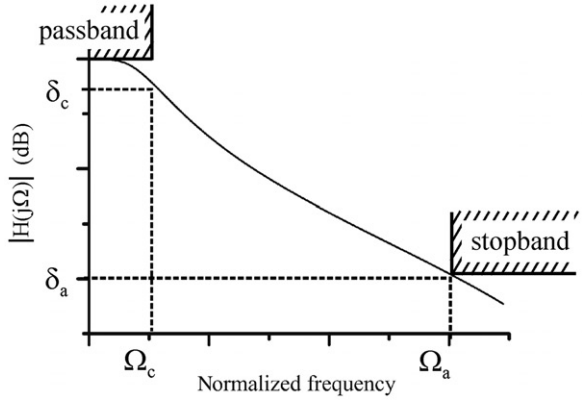

Figure 1. Modulus of the transfer function and relevant parameters for a general low-pass filter.

This defines the passband, for frequencies lower than Ω_c, and the stopband, for frequencies higher than Ω_a. Figure 1 shows a typical shape for the modulus of the complex transfer function $H(j\Omega)$ for such a filter.

In digital filter design, filters of this type may be implemented using the Butterworth, Chebyshev or elliptical filter approaches. However, only the Butterworth approach is monotonic (without undulations in the gain of the filter) over the passing and attenuated frequency ranges. Furthermore, unlike the other filter families, Butterworth filters introduce a change in the phase of the input signal which is smooth and continuous, which becomes an advantage for our application.

A typical Butterworth filter has a transfer function $H(j\Omega)$ with a modulus expressed as

$$\left|H(j\Omega)\right|^2 = \frac{1}{1+(j\Omega/\Omega_c)^{2N}}, \tag{1}$$

where j is the imaginary constant, Ω is the frequency of the incoming signal and Ω_c is the cut-off frequency of the filter. N is the order of the filter and controls the steepness of the transfer function after the cut-off frequency. Obviously, the lowest-order filter capable of properly filtering the signal is the optimum solution in computational terms.

Here we would like to stress the difference between the phase data to be extracted from the fringe pattern after a phase extraction process is applied, and the change in phase of the input signal introduced by the filter. In the approach we are using, changing the phase of the incoming signal implies a displacement of the position of the fringes, which is a highly undesirable feature for the filter being applied. A null phase change in the incoming signal data is a requirement for accurate phase reconstruction. In digital filter design,

such fringe displacement is related to the group delay $\tau(\Omega)$ introduced by the filter, defined as

$$\tau(\Omega) = -\frac{\mathrm{d}(\arg H(j\Omega))}{\mathrm{d}\Omega}. \tag{2}$$

2.2. Parameter selection

Thus far, only the continuous frequency domain (Ω) has been considered. However, the signal will be spatially sampled, so we need to design a filter in the discrete frequency domain (ω). The central parameters for filter selection are the discrete cut-off frequency (ω_c) and the minimum attenuated frequency (ω_a), together with their respective attenuations δ_c and δ_a. A FFT algorithm is used to detect the dominant frequencies in the signal, so a ω_c value can be obtained from a weighted sum of all frequencies with contributions above the noise threshold. This spatial frequency is then normalized to the Nyquist frequency of the fringe pattern image. Following the usual criteria in digital filter design, δ_c is set at $-3\,\mathrm{dB}$, which is the typical gain change assumed in the passing frequencies, and δ_a is set at $-25\,\mathrm{dB}$, which is the value that filters a maximum 8-bit input signal to a non-detectable value. The minimum attenuation frequency ω_a is then determined through

$$N = \frac{\log\left[\frac{10^{-0.1\delta c}-1}{10^{-0.1\delta a}-1}\right]^{1/2}}{\log\frac{\omega_c}{\omega_a}} \tag{3}$$

by imposing $N=2$, which yields a second-order Butterworth filter. As shown below, such a low order filter is sufficient to properly process very complex fringe patterns.

2.3. Transfer function in the continuous domain

In the last paragraph we have set the filter parameters in the discrete frequency domain. However, it is preferable to design the filter in the continuous domain. The bilinear transform establishes bidirectional correspondence between the continuous and discrete frequency spaces through

$$s = \frac{2}{T_{sample}}\frac{z-1}{z+1}, \tag{4}$$

where $s = j\Omega$ and $z = e^{j\pi\omega}$. T_{sample} is the spatial period of the sampling of the signal. Since we will use this transform bidirectionally from one space to the other throughout the design procedure, T_{sample} will be canceled out and may be neglected. Equation (4) may be rewritten as

$$\Omega = \frac{2}{T_{sample}}\, tg\left(\frac{\pi}{2}\omega\right), \tag{5}$$

so we may calculate the continuous domain cut-off frequency Ω_c using Equation (5) and the ω_c value previously determined in the discrete frequency domain.

The transfer function of a second-order Butterworth filter in the continuous frequency domain has been established as

$$H(s) = \frac{k\cdot\Omega_C^2}{s^2 + 2\xi\Omega_C s + \Omega_C^2}, \tag{6}$$

where k is the gain of the filter and ξ is the damping in the gain. By establishing $k=1$ and $\xi=\sqrt{2}$, we ensure that the gain values stay below 1 in all passing frequencies. Thus, once the FFT is applied to one line in the fringe pattern, and Ω_c is fixed as a weighted combination of all frequencies above the threshold, the transfer function of the filter in the continuous domain becomes known. In addition, Equation (6) shows that all coefficients of the polynomial are positive, so its roots have a negative real part, which ensures the stability of the filter response.

2.4. Discrete domain implementation

As the signal is sampled, the discrete domain equivalent of the transfer function in Equation (6) must be determined. By again applying the bilinear transform of Equation (4) in Equation (6), we get

$$H(z) = \frac{\Omega_C^2/4}{\left(\Omega_C^2/4 + \xi\Omega_C + 1\right)}\cdot\frac{(z+1)^2}{\left\{\begin{array}{c} z^2 + \left(\frac{\Omega_C^2/2-2}{\Omega_C^2/4+\xi\,\Omega_C+1}\right)z \\ +\left(\frac{\Omega_C^2/4-\xi\,\Omega_C+1}{\Omega_C^2/4+\xi\,\Omega_C+1}\right)\end{array}\right\}}. \tag{7}$$

It may be noticed how the result depends only on the continuous cut-off frequency Ω_c, so determining the transfer function is straightforward once the Ω_c value is known.

The response of the designed family of filters in modulus and phase is very similar regardless of the ω_c value used, provided that it stays within reasonable limits. Only minor changes in the appearance of the plots may be appreciated. Figure 2 shows the filter obtained for a typical cut-off value ($\omega_c = 0.09$), where the modulus plot shows the desired attenuations of $-3\,\mathrm{dB}$ at $\omega_c = 0.09$ (Figure 2(*a*)) and $-25\,\mathrm{dB}$ at $\omega_a = 0.35$. The slope of the filter is not sharp, due to the low order used. Figure 2(*b*) shows the phase of the filter, showing the nonlinearity of the phase of the filter with frequency.

As a consequence of the nonlinearity of the phase of the filter shown in Figure 2(*b*), the group delay plot (Figure 2(*c*)) shows a delay of 5 to 6 samples

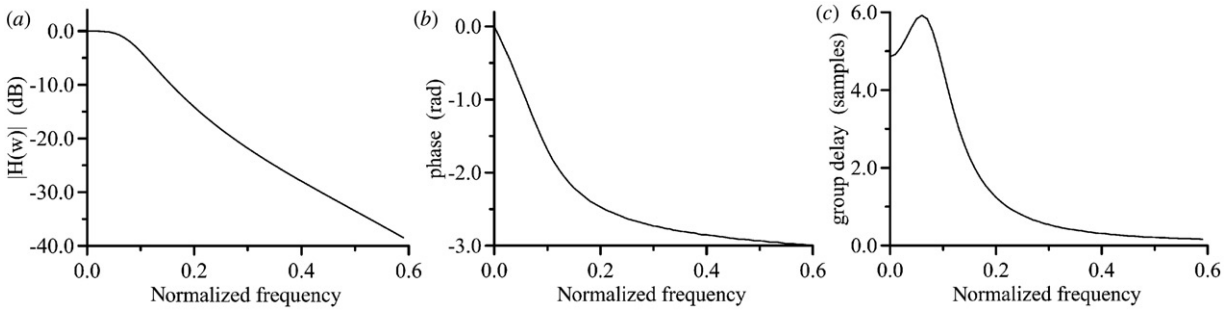

Figure 2. Behavior of the filter for a typical cut-off frequency value of $\omega_c = 0.09$: (*a*) modulus of the filter in dB against normalized frequency; (*b*) phase in degrees against normalized frequency; (*c*) group delay in samples against normalized frequency. The behavior of the filter for other ω_c values used in fringe pattern analysis was equivalent.

introduced in the phase of the incoming signal for the passing frequencies. As mentioned, in fringe pattern analysis, this means that the fringe is displaced 5 or 6 pixels from its original location, which is totally unacceptable. This drawback is overcome by filtering each row or column of the fringe pattern in opposite directions. The phase change in the ''right to left'' filtering is compensated by the 'left to right' one, thus canceling out the effect of the phase delay. It is worth mentioning that this double-pass procedure enables the use of a Butterworth filter of a very low order ($N = 2$).

2.5. *Discrete domain implementation*

Finally, the discrete domain transfer function of the filter is converted to an equation in differences through a new mathematical transformation called the z-transform, which yields the final equation of the filter to be implemented as

$$\begin{aligned} Y(k) = {} & \frac{\Omega_C^2/4}{(\Omega_C^2/4 + \xi\Omega_C + 1)} X(k) \\ & + \frac{2\Omega_C^2/4}{(\Omega_C^2/4 + \xi\Omega_C + 1)} X(k-1) \\ & + \cdots + \frac{\Omega_C^2/4}{(\Omega_C^2/4 + \xi\Omega_C + 1)} X(k-2) \\ & - \frac{(\Omega_C^2/2 - 2)}{(\Omega_C^2/4 + \xi\Omega_C + 1)} Y(k-1) \\ & + \cdots - \frac{(\Omega_C^2/4 - \xi\Omega_C + 1)}{(\Omega_C^2/4 + \xi\Omega_C + 1)} Y(k-2). \end{aligned} \quad (8)$$

The coefficients of the transfer function stay the same as in Equation (7). The exponents of the z term have adopted the order of the spatial samples of the input function $X(k)$. Thus, z^{-1} becomes $X(k-1)$, the sample before the one being considered in the input function. Likewise, $Y(k-2)$ is the sample of the filter output function taken two samples before the one being considered, which implies a recursive output.

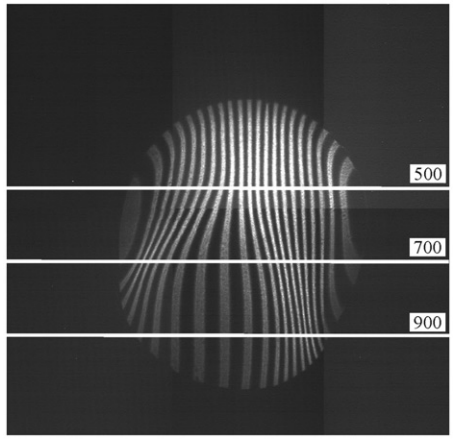

Figure 3. Fringe pattern to be processed, highlighting the fringe pattern lines at rows 500, 700 and 900 in the fringe-pattern image, which will be analyzed in detail in the following figures.

Unlike classical morphological smoothing, our approach uses the spatial frequencies of the signal to fix the optimum coefficients for the transfer function, which is valid regardless the distribution of spatial frequencies present in the signal. Furthermore, values from both the sampled input function $X(k)$ and the sampled output signal $Y(k)$ are used. Additionally, Equation (8) is very easily implemented in software applications of any platform with a very low computational cost, thanks to the low order used in the filter.

3. Application to complex ronchigram processing

The adaptive filter designed will be used for phase extraction of the fringes in a complex fringe pattern obtained using a digital Ronchi deflectometry setup (Figure 3(*a*)) [13]. Such a fringe pattern is obtained

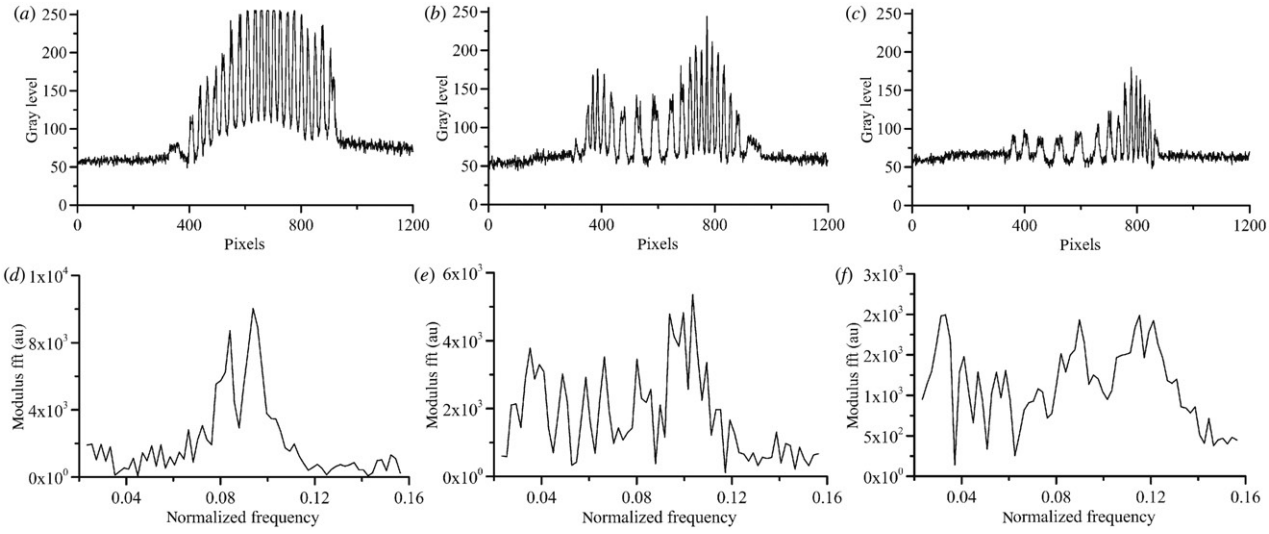

Figure 4. The upper row shows the intensity profile plots corresponding to the lines highlighted in Figure 3: (*a*) signal in line 500; (*b*) signal in line 700; (*c*) signal in line 900. The bottom row shows the modulus of the FFT for the corresponding signal in the upper row: (*d*) modulus of FFT of line 500; (*e*) modulus of FFT of line 700; (*f*) modulus of FFT of line 900. Fringes are seen to be strongly non-monochromatic, with a number of different frequencies yielding very relevant contributions, especially in rows 700 and 900.

using a collimated beam that crosses a progressive ophthalmic lens with a distance power of +3.0 D and an addition of +3.0 D. The near vision area is in the lower side of the image. The resulting wavefront crosses a Ronchi ruling with a frequency of $0.5\,\mathrm{mm}^{-1}$ and a square-wave transmittance profile. The full-sized ronchigram is registered in an array of independent 2×3 CCD cameras with overlapping image areas. The composed image measures 1200×1170 pixels and is acquired from behind a diffusive screen, so it has a significant noise level [14], plus a number of diffractive features introduced by the ruling. The important power increment in the lens yields a strongly non-monochromatic fringe-pattern. The stitching image areas may be appreciated at some borders in Figure 3(*a*). In both the fringes and the bias, the illumination levels vary from one region of the image to the next, so it cannot be processed using conventional algorithmics without causing significant accuracy losses.

3.1. Fringe-pattern analysis

The horizontal white lines in Figure 3 are the pixel rows which will be used as the signals to be analyzed in detail in the following. It may be noticed how variable spatial frequency distributions, fringe profile shapes and background noise levels are present in the signal to be processed. The intensity profile along each of the white lines in Figure 3 is presented in the upper row of Figure 4 (i.e. Figure 4(*a*)–(*c*)). The changes in amplitude in the Fourier transform profile with frequency of the signals are presented in the bottom row of Figure 4 (Figure 4(*d*)–(*f*)), correspondingly. The plots show the different situations which are found in this particular fringe pattern, but which are tackled using the same filtering strategy described. From the plots, the non-feasibility of using a single frequency for FFT filtering without losing a significant amount of data becomes evident.

The Ω_c value for each line is obtained using a weighted sum which assigns to each frequency with amplitude of the FFT above the noise threshold a weight proportional to its relative amplitude. Once Ω_c is known, it is used to define the coefficients of the filter according to Equation (8). Typical Ω_c values obtained stay in the interval from 0.02 to 0.1.

The obtained filter is then applied to each of the lines in both directions, in order to compensate for the known phase delay introduced by the filter. Figure 5 depicts the results of the described filtering strategy. The upper line of subplots (Figure 5(*a*)–(*c*)) shows the results obtained once the double-pass filtering strategy has been applied to the signals presented in Figure 4(*a*)–(*c*). The bottom line of Figure 5 shows a detail of the corresponding filtered signal in the upper row. In each of the subfigures in the bottom row, we simultaneously present the original signal (dotted line), the filtered signal after the first pass of the filter (thin solid line), which shows the effect of group delay effect in the form of an undesired displacement in the

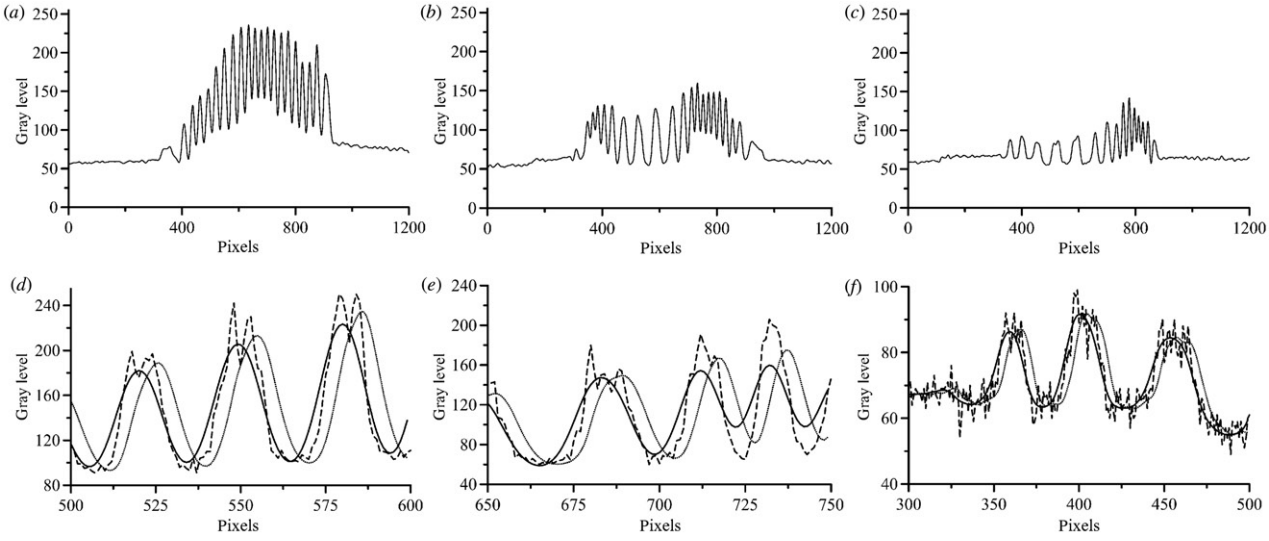

Figure 5. Complete filtered signal (top row) and detail of filtered fringes (bottom row) for: (*a*) signal in line 500; (*b*) signal in line 700; (*c*) signal in line 900. Below each of the filtered signals we present a detail of the signal including the original signal (dotted line), the filtered signal after the first pass (thin solid line), which shows fringe displacement by the effect of group delay, and the filtered signal after applying the filter twice in both directions (thick solid line), without group delay.

position of the fringes, and the final filtered signal after applying the filter twice in both directions (thicker solid line), without any displacement in the position of the fringes. Notice the quasi-sinusoidal profile of the fringes which is obtained for all spatial frequencies in a same signal, which enables phase-shifting algorithms to be applied accurately.

3.2. *Phase extraction*

In order to validate the usefulness of the filtering strategy in a noisy and complex fringe pattern, a simple phase-shifting strategy was implemented in the setup. With this purpose, we have implemented the classical Carré phase shifting algorithm [2], although a number of different phase-shifting algorithms have been already proposed to cope with different metrological specifications, and could have been also selected. In the Carré algorithm, four fringe patterns which are phase-shifted an arbitrary value α are combined to accurately recover the phase of the sampled wavefront, using

$$\Phi(x,y) = \tan^{-1}\left(\frac{\left\{\begin{array}{l}[I_2(x,y) - I_4(x,y)]\\ \quad +[I_1(x,y) - I_3(x,y)]\end{array}\right\}}{\left\{\begin{array}{l}[I_2(x,y) - I_4(x,y)]\\ \quad -[I_1(x,y) - I_3(x,y)]\end{array}\right\}}\right), \qquad (9)$$

where $I_i(x,y)$ is the intensity of the pixel at position (x,y) after the $(i-1)$th phase shift. An α value of $\frac{1}{2}\pi$ was selected.

Four phase-shifted fringe patterns corresponding to ronchigrams obtained using the progressive ophthalmic lens described in the previous subsection were acquired and filtered using the strategy presented along this work, and the phase map was recovered. The wrapped phase map obtained using the proposed technique is presented in Figure 6(*a*). The wrapped phase data obtained when applying the Carré algorithm onto ronchigrams filtered using a non-adaptive smoothing procedure (classical three-pixel averaging) is presented in Figure 6(*b*). It may be shown how the proposed strategy obtains more accurate phase values. This is easily observed in the figures in the shape of artifacts in the largest phase values, although deviations occur in the whole phase range. The comparison of both filtering strategies for a single phase cycle is presented in more detail in Figure 7, showing the difference in phase values obtained. The average difference in the phase values obtained is typically of some tenths of milliradians, with maximum difference values exceeding 150 mrad in the worst cases.

4. Conclusions

A general, quick, computationally efficient and robust approach to fringe pattern processing based on digital filter design theory is presented that allows phase extraction out of noisy ronchigrams with high accuracy. The filter design details presented allow the filter to be expressed as an equation of differences that depends only on the cut-off frequency selected. The cut-off frequency of the filter in each pixel row (or column) of the fringe pattern is calculated as

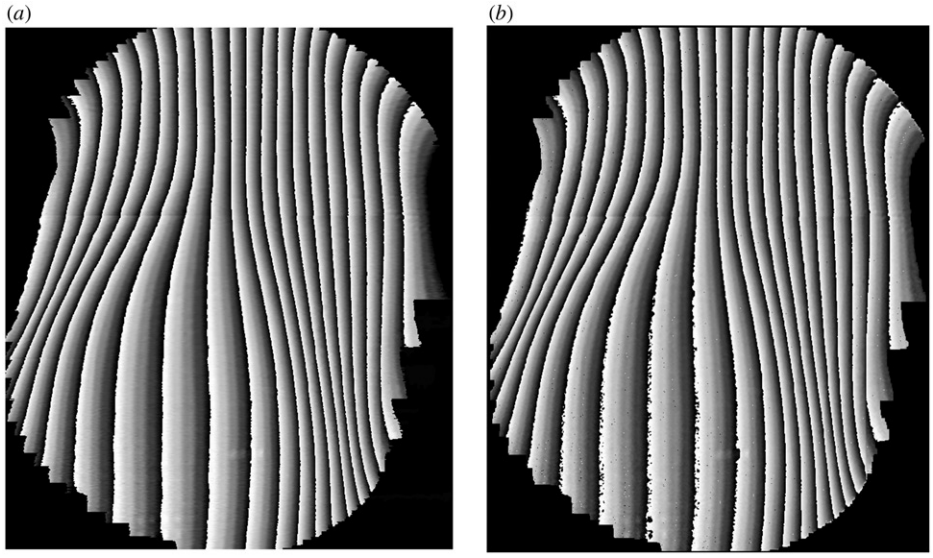

Figure 6. Phase information recovered from the Carré algorithm after four phase-shifted ronchigrams with the described lens: (*a*) using the adaptive filtering strategy proposed here; (*b*) using non-adaptive averaging. Artifacts are visible in the largest phase values, although errors are present for all phase values.

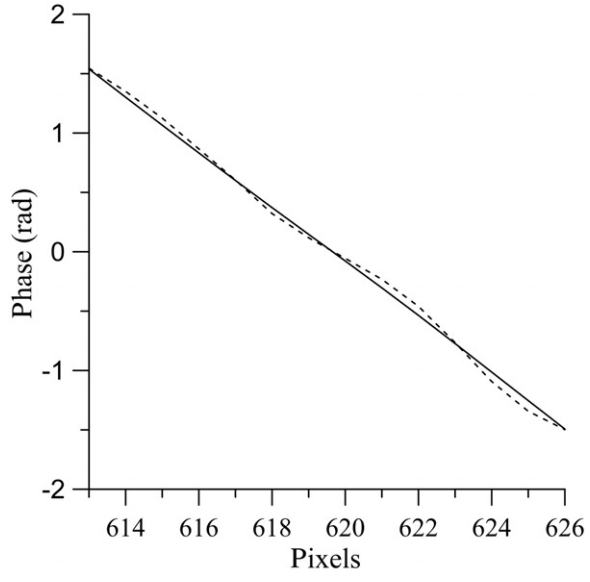

Figure 7. Comparison of phase values obtained using two different filtering strategies. Phase values obtained with the adaptive filtering strategy (solid line) are compared with phase values obtained using a non-adaptive frequency filter (three-pixel averaging, dashed line).

a weighted sum using the relative amplitude of the FFT for each of the frequencies above a given threshold. The modulus, phase and group delay of this second-order Butterworth filter were presented and discussed. The double-pass strategy used to compensate for fringe displacement was shown to enable the use of a filter of very low order ($N=2$). In addition, the filter was formulated in the shape of an equation in differences, resulting in an implementation with a very low computational cost. The described strategy was then applied to phase extraction in an experimental fringe pattern from a progressive addition lens obtained through a digital Ronchi deflectometry setup, by use of the Carré algorithm. The filter has been shown to perform equally well under the different conditions found in the image, although very different frequency distributions and noise levels were present in the fringe-patterns. It was demonstrated that this simple approach could be of great interest for automated fringe pattern processing, especially when noisy and complex fringe patterns are involved.

Acknowledgements

The authors wish to thank Spanish Ministry of Science and Innovation for projects FIS2008-05071, DPI2009-13379 and DPI2011-25525.

References

[1] Gasvik, K.J. *Optical Metrology*, 2nd ed.; John Wiley & Sons: Chichester, UK, 1996.
[2] Creath, K. *Prog. Opt.* **1988,** *26,* 349–393.
[3] Takeda, M. *Ind. Metrol.* **1990,** *1,* 79–99.
[4] Cornejo-Rodríguez, A. *Optical Shop Testing*, 3rd ed.; John Wiley and Sons: New York, 2007.
[5] Royo, S. Topographic Measurements of Non-rotationally Symmetrical Surfaces Using the Ronchi Test. Ph.D. Dissertation, UPC-BarcelonaTech, Terrassa, Spain, 1999.

[6] Malacara, D.; Servín, M.; Malacara, Z. *Interferogram Analysis for Optical Testing*; Marcel Dekker: New York, 1998.
[7] Takeda, M.; Ina, H.; Kobayashi, S. *J. Opt. Soc. Am.* **1982,** *72,* 156–160.
[8] Qian, K.; Soon, S.H. *Opt. Eng.* **2005,** *44,* 075601.
[9] Sciammarella, C.A.; Kim, T. *Opt. Eng.* **2003,** *42,* 3182–3193.
[10] Zhong, J.; Weng, J. *Appl. Opt.* **2004,** *43,* 4993–4998.
[11] Qian, K.; Gao, W.; Wang, H. *Appl. Opt.* **2008,** *47,* 5420–5428.
[12] Li, S.; Chen, W.; Su, X. *Appl. Opt.* **2008,** *47,* 3369–3377.
[13] Arasa, J.; Royo, S.; Pizarro, C. *Appl. Opt.* **2000,** *39,* 5721–5731.
[14] Caum, J. Characterization of Densely Sampled Wavefronts. Ph.D. Dissertation, UPC-BarcelonaTech, Terrassa, Spain, 2010.
[15] Oppenheim, A.V.; Schafer, R.W.; Buck, J.R. *Discrete-time Signal Processing*, 2nd ed.; Prentice Hall: New York, 1999.
[16] Ogata, K. *Discrete-time Control Systems*, 2nd ed.; Prentice Hall: New York, 1994.
[17] Phillips, C.L.; Nagle, H.T. *Digital Control Systems: Analysis and Design*; Prentice Hall: New Jersey, 1984.